Applied Geochemistry 158 (2023) 105779

Contents lists available at ScienceDirect

Applied Geochemistry

journal homepage: www.elsevier.com/locate/apgeochem

Targeting oxidation sites on boreal acid sulfate soil macropore surfaces mitigates acid and metal release to recipient water streams

Eva Högfors-Rönnholm [a,*], Pekka Stén [b], Stephan Christel [c,1], Sören Fröjdö [d], Tom Lillhonga [a], Paweł Nowak [e], Peter Österholm [d], Mark Dopson [c], Sten Engblom [a]

[a] Research and Development, Novia University of Applied Sciences, 65200, Vaasa, Finland
[b] Environmental Technology, Vaasa University of Applied Sciences, 65200, Vaasa, Finland
[c] Centre for Ecology and Evolution in Microbial Model Systems (EEMiS), Linnaeus University, 39231, Kalmar, Sweden
[d] Department of Geology and Mineralogy, Åbo Akademi University, 20500, Turku, Finland
[e] Jerzy Haber Institute of Catalysis and Surface Chemistry, Polish Academy of Sciences, 30239, Kraków, Poland

ARTICLE INFO

Editorial handling by Qusheng Jin

Keywords:
16S rRNA gene
Boreal soil microbial community
Calcium carbonate
Metal laden acidic waters
Peat
Sulfide oxidation

ABSTRACT

When reduced sulfidic parent sediments are oxidized, they become acid sulfate soils and discharge metal laden acidic solutions that can damage the environment, infrastructure, and human health. Consequently, methods to mitigate the effect of acid sulfate soils are a priority in affected areas. In this study, acid sulfate soil core samples, consisting of a natural network of preferential-flow soil macropores with defined macropore surfaces and inner cores of denser clay, were characterized and subjected to treatments with calcium carbonate and peat suspensions, or combinations thereof. The effects on the geochemistry and microbial communities were examined on both macropore surfaces and in inner cores. Although transport of treatment substances into the inner cores was demonstrated, no substantial effects were found on the geochemistry and microbial community that consisted of bacterial taxa commonly identified in acid mine drainage. In contrast, positive treatment effects were clearly detected on macropore surfaces and the most promising mitigation effects were detected for treatments combining calcium carbonate and peat suspensions. These treatments increased the pH of the macropore surfaces, added an electron donor in the form of peat, and significantly decreased the relative abundance of acidophilic bacterial populations while shifting the microbial community towards species typically growing at circumneutral pH values. These new environmental conditions were favorable for iron reduction that resulted in a positive effect on permeate quality. The study presents novel data regarding the important differences between acid sulfate soil macropore surfaces and inner cores, as well as their diverse biogeochemical characteristics. It further establishes that the major oxidation-reduction processes occur at the macropore surfaces, and that the combination treatment was the most effective at mitigating the negative environmental effects.

1. Introduction

Coastal areas in Finland are often characterized by fine-grained Holocene marine sediments that form pH-neutral black soil material (termed sulfidic soil material or 'potential acid sulfate soil' material; PASS) with a high clay and sulfur content and very low hydraulic conductivity. The PASS can become exposed to air and subsequently oxidized due to drainage by post-glacial isostatic land uplift and/or artificially for agricultural and infrastructure uses (Yli-Halla et al., 2017). In consequence, it is converted into a sulfuric soil material, often termed an actual 'acid sulfate soil' (ASS), that is characterized by low pH and the release of toxic metals including cadmium, nickel, and aluminum (Wu et al., 2013). If these acidic, metal-laden waters reach rivers and ultimately the Baltic Sea (Nordmyr et al., 2008; Roos and Åström, 2006), they can cause severe damage to the environment (Sullivan et al., 2002) and are hazardous to human health (Hinwood et al., 2006).

As PASS is drained, largely irreversible soil shrinkage occurs. This leads to the formation of a permanent structure of cracks and other macropores (e.g., Johnston et al., 2009) that are prerequisites for the

* Corresponding author.
E-mail address: eva.hogfors-ronnholm@novia.fi (E. Högfors-Rönnholm).
[1] Present address: Cemvita Factory, 8300 Alcott St., Westminster, Colorado, USA.

https://doi.org/10.1016/j.apgeochem.2023.105779
Received 2 May 2023; Received in revised form 23 August 2023; Accepted 29 August 2023
Available online 30 August 2023

rapid development of an ASS. The formed network of soil macropores (consisting of interconnected cracks and tubular macropores) leads to a preferential flow pattern with a high hydraulic conductivity and serves as the basis for the very efficient drainage of these soils. It also allows penetration of air into the soil that ultimately results in the transformation of the metal (mainly iron) sulfide-rich PASS into ASS (Johnston et al., 2009). As the sulfide oxidation proceeds, the produced sulfuric acid lowers the pH and allows iron and sulfur oxidizing acidophiles (optimum growth pH < 5) to become active and further catalyze the transition from PASS to ASS by regenerating ferric iron and oxidizing sulfur compounds to sulfuric acid (Wu et al., 2013). The importance of the preferential-flow macropore surfaces is evident in that they are the sites where a reactant such as oxygen is made available during dry periods and thus, promotes the microbiological processes. At these surfaces, reaction products and leached substances can either form precipitates or enter a percolating water flow for further transport away from the reaction sites and eventually exit the soil during wet seasons. This cycle of introduction of reactants and removal of products drives the decades-long process that eventually exhausts the sulfuric soil material of oxidizable sulfides (Österholm and Åström, 2004; Virtanen, 2015).

The soil material in a structured ASS consists of solid columnar blocks of which the outer walls form surfaces of macropores. A macropore surface is a highly porous and both physically and chemically a highly heterogeneous environment with surfaces often lined with iron oxyhydroxide and/or oxyhydroxysulfate minerals (Dent, 1986). The solid blocks, the inner parts of which are called inner cores in this work, consist of dense clay material. In a mature ASS in agricultural use, two very different modes of transport can therefore be expected. Above or at the drainage depth, a high hydraulic conductivity allows soil solution and solutes to be quickly transported through the network of preferential-flow macropores and further on to drainage channels (Johnston et al., 2004). In contrast, a much slower mode of transport is encountered in the inner cores. Here transport of solutes is by diffusion, if the microstructure is water-filled, or by film boundary transport as part of a rewetting process if the microstructure has dried out (Yong, 2003). Differences in the combined chemical and microbiological characteristics between the boreal ASS inner core soil materials versus the macropore surfaces, and the implications regarding acid and metal release, have not been comprehensively investigated.

Attempts to mitigate the release of metal laden acidic waters from ASS have focused on the introduction of chemicals to raise the pH in order to inactivate acidophilic iron and sulfur oxidizing bacteria and/or to provide a carbon and energy source to promote iron and sulfate reducing microorganisms that generate e.g., sulfide to immobilize the metals (Michael et al., 2015; Dang et al., 2016; Kölbl et al., 2018). These studies include the addition of calcium carbonate suspensions utilizing a subsurface drainage system and preferential-flow soil macropores to reach far into a boreal ASS (Dalhem et al., 2019; Wu et al., 2015). These treatments increase the drainage water pH and decrease metal leaching for up to four years after treatment (Dalhem et al., 2019). Mixing dry ultrafine-grained calcium carbonate into homogenized ASS further inactivates acidophilic bacteria inhabiting the boreal ASS by increasing the pH of the soil (Högfors-Rönnholm et al., 2018a). Mixing both calcium carbonate and an organic material in the form of peat into the boreal ASS decreases metal and acid release, increases the overall microbial diversity of the soil, and reactivates an iron reducing bacterial population (Högfors-Rönnholm et al., 2020). However, how pumping a mitigation suspension through the boreal ASS preferential-flow soil macropores affects the diverse biogeochemical characteristics of the macropore surfaces and inner cores separately has not been investigated.

This study utilized laboratory column experiments to investigate the biogeochemical characteristics of boreal ASS macropore surfaces and inner cores and how different mitigation suspensions affect these soil environments as well as the soil drainage water. The tested hypothesis was that the exposed surfaces in the network of boreal ASS preferential-flow macropores were the main sites for the chemical and microbiological oxidation processes.

2. Materials and methods

2.1. Field site and soil sampling

The Risöfladan experimental field is situated on the Baltic Sea coast in Vaasa, western Finland (63°02′50″ N, 21°42′42″ E). The old marine sediments of Risöfladan were drained over 60 years ago and have since developed into a typical clay-type, extensively cracked ASS (Fig. 1a) with an organic matter content of approximately 5% (Högfors-Rönnholm et al., 2018a). Details of the study area and the soil physicochemical parameters at the experimental field (the site is often called Mustasaari) have been previously reported (Nordmyr et al., 2006; Åström et al., 2007; Boman et al., 2008; Wu et al., 2013) and the classification of the soil has been discussed by Joukainen and Yli-Halla (2003). Soil core samples were collected from the field according to Högfors-Rönnholm et al. (2018a) when the groundwater table in the soil was high. Briefly, polyethylene tubes were pushed into the ground by an excavator (Fig. S1), lifted, sealed airtight, and stored at 4 °C until used in the experiments.

2.2. Treatment substances and preparation of suspensions

The substances used in the ASS mitigation experiments were the same as those used by Högfors-Rönnholm et al. (2018a, 2020) and in field studies by Dalhem et al. (2019). The suspensions must be stable and therefore ultrafine-grained substances were used. They were: 'C2', an ultrafine-grained calcium carbonate ($CaCO_3$) with a median particle diameter of 2.5 μm (C2, Nordkalk Corporation); 'EB', an aqueous suspension (Enrich Bio, Nordkalk Corporation) of 37% ultrafine-grained $CaCO_3$ with a median particle diameter of 0.3 μm that includes the dispersing agent Alcoguard® H 5941 (4% per dry weight of $CaCO_3$, Akzo Nobel); 'P', a fine-grained peat of biodegradation level H1 (the least biodegraded fraction according to the von Post scale (Andriesse, 1988)) with a median particle diameter of 20 μm and a typical organic content of 95–98% (Vapo Fibers); 'C2–P' refers to a treatment with C2 $CaCO_3$ followed by a treatment with peat; and 'EB-P' refers to a treatment with Enrich Bio $CaCO_3$ followed by a treatment with peat. The C2 product has previously been tested for mitigation of ASS in a column experiment (Wu et al., 2015) and in field experiments (Dalhem et al., 2019), while the C2, Enrich Bio, and H1 peat products were investigated with homogenized ASS (Högfors-Rönnholm et al., 2018a, 2020).

To avoid microbial contamination, the MilliQ-ultrapure water was autoclaved, cooled to 10 °C in closed containers, and kept closed until used. As a consequence of the autoclaving, the oxygen content of the water was reduced by about 20% at the beginning of the experiments and in unstirred containers the concentration was slowly restored by diffusion throughout the experiment. For treatments with C2 and EB, 8 g L^{-1} $CaCO_3$ was suspended in 15 L water with stirring in an open container. The P treatments used 4 g L^{-1} peat for the suspensions, likewise with stirring in an open container. The suspensions for the C2–P and EB-P treatments were made separately with 4 g L^{-1} $CaCO_3$ and 1 g L^{-1} peat in a similar manner. Pilot studies were used to determine maximum concentrations without blocking the preferential-flow soil macropores. In the case of combined treatments, the $CaCO_3$ suspension was applied before the peat suspension. For the control soil cores ('C'), only autoclaved MilliQ-ultrapure water was used. All suspensions were prepared immediately before use in the experiments.

2.3. Experimental procedure

The experimental procedure was according to Wu et al. (2015) with some modifications. Briefly, soil cores were cut at the oxidized soil layer

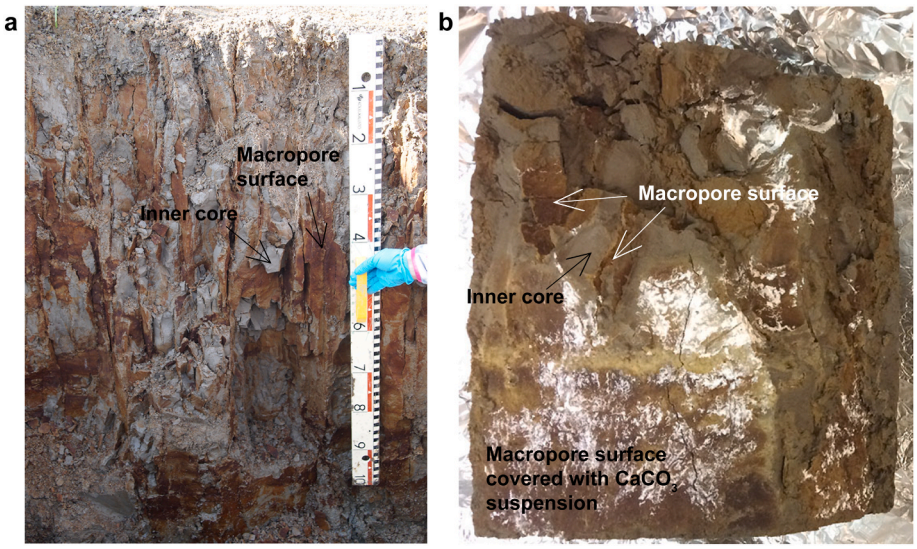

Fig. 1. Photographs of the heterogenic and cracked structure of a boreal acid sulfate soil with macropores consisting of interconnected cracks, fissures, and tubular pores and an inner core of denser clay. Images taken in the field (a) and from a split soil core (approximately 14 × 15 cm) treated with calcium carbonate suspension (b).

at a depth of 70–85 cm below ground level that was rich in preferential-flow soil macropores, the core was inserted into a rubber membrane, and placed into the column. After filling the column with water and applying an external pressure to prevent bypass flow between the rubber membrane and the soil core, a diaphragm pump (Grundfos DME or DDA) was used to pump from the bottom of filled 15-L recently-open containers: (i) an initial flushing phase with approximately 10 L of unstirred autoclaved MilliQ-ultrapure water at a constant flow of 100 mL h^{-1}; (ii) a treatment phase with approximately 10 L of unstirred autoclaved MilliQ-ultrapure water for the control cores (C), approximately 10 L of constantly stirred treatment suspension for single treatment cores (C2, EB), approximately 10 L + 10 L of constantly stirred treatment suspensions for combined treatments (C2–P, EB-P, where the $CaCO_3$ suspension was applied before the peat suspension) at 50 mL h^{-1}; and (iii) a final flushing phase with approximately 10 L of unstirred autoclaved MilliQ-ultrapure water at 50 mL h^{-1}. The initial flushing phase was used to remove accumulated oxidation reaction products from the preferential-flow soil macropores before treatment and the final flushing phase was used to mobilize the remaining suspension and to reach a new steady state after treatment. All experiments were performed in duplicates using separate soil cores and conducted at 10 °C with pre-tempered water and treatment suspensions. This temperature is the average temperature for the soil layer at 70–85 cm below ground level (Wu et al., 2013) and has also been used in previous experiments (Högfors-Rönnholm et al., 2018a, 2020). Separate suspensions were used for the two replicates (Fig. S2). After the final flushing phase, the soil cores enclosed by the rubber membranes were removed from the column apparatus, wrapped in aluminum foil, sealed tightly in plastic bags to limit oxidation reactions, and incubated for 4 weeks at 10 °C in the dark. The incubation was used to allow time for also relatively slow processes, e.g., diffusion, to yield measurable effects of the treatments.

2.4. Permeate analyses

The permeate (i.e., the solution emanating from a soil core sample during the experiment) represents drainage water under field conditions and was analyzed during the experiment. Temperature, pH, temperature-corrected (25 °C) conductivity (σ), and oxidation-reduction potential (ORP) versus an Ag/AgCl/KCl (3.5 M) reference electrode were measured using an YSI Professional Plus instrument (YSI Inc.) and a flow-through cell (Quatro Cable Flow Cell, YSI Inc.). The measured ORP values were converted to Eh, i.e., potentials versus the standard hydrogen electrode (SHE), according to Eh = E (measured ORP) + E (reference electrode vs SHE). Bates (1973) lists standard potentials for the Ag/AgCl/KCl (3.5M) electrode at different temperatures and at 10 °C it is Eh = E (measured ORP) + 215 mV. The presence of dissolved oxygen in the measurements was likely not a concern as Nordstrom et al. (1979) show that the Eh in stream waters saturated with dissolved oxygen, in the presence of electroactive iron species, is determined by the ferrous-ferric ratio. Sub-samples of permeates were collected twice a day for multi-element analysis with inductively coupled plasma optical emission spectrometry (ICP-OES) at Activation Laboratories LTD, Canada and determination of sulfate concentrations by ion chromatography (Dionex ICS 1100).

2.5. Treated soil core analyses

2.5.1. Sampling

The soil cores were split open by hand after the four-week incubation (Fig. 1b) and macropore surfaces plus inner cores were sampled aseptically by carefully scraping surfaces and inner cores with a spatula. For geochemical soil extract analyses, two tubes each of 15 g soil were taken from the macropore surfaces and from the inner cores and stored at −20 °C until analysis. For microbial community analyses, two 50 mL tubes were half filled with soil taken from the macropore surfaces of each soil core and two tubes from the inner cores. DNA was extracted immediately after sampling (described below). Excess soil samples from microbial analyses were used for estimation of dry weight (SFS-EN 12880). The remaining soil cores were stored at −20 °C with limited access of air and used for energy dispersive x-ray fluorescence (XRF) analysis.

2.5.2. Geochemical soil extract analyses

Soil samples were stored in 50 mL tubes filled with deoxygenated MilliQ-ultrapure water at a sediment-water (wet weight) ratio of 1:2.5, agitated with a Vortex for 1 h, and centrifuged (2000 g, 10 min). The extract (25 mL) was filtered (0.2 μm) and divided into aliquots for the analysis of conductivity, Fe^{2+}, and SO_4–S. pH was measured in the remaining unfiltered undisturbed extract with a Hamilton Flatrode electrode. Due to the risk of oxidation, Fe^{2+} was immediately analyzed using the 1,10-phenanthroline method based on Fadrus and Malý (1975) and Högfors-Rönnholm et al. (2018a). This method incorporates the use

of NTA (nitrilotriacetic acid) for forming complexes with ferric iron and thus stabilizing the balance between ferric and ferrous iron. Sulfur in the extract was measured as SO_4–S by ion chromatography by Lounais-Suomen Vesi Oy, Turku, Finland. To account for dilution effects, the results were normalized against soil dry weight. The total amount of Fe^{2+} and SO_4–S in the extract were calculated by multiplying the concentrations with the total amount of water (including pore water) and thereafter normalized against soil dry weight. Conductivity in the extract was corrected to represent the average extract/dry weight ratio (5.0) assuming a linear relationship between conductivity and dilution.

2.5.3. XRF analysis

Frozen samples from macropore surfaces and inner cores from each soil core were analyzed under vacuum by macro-XRF analysis (EDX 3600H Alloy Analyzer, Skyray Instruments, USA). Macropore surface areas covered with visible $CaCO_3$ deposits (Fig. 1b) were avoided as thick deposits would attenuate X-ray fluorescence from beneath the calcite layer. As a reference, at least one inner core sample from each soil core was prepared by cutting a piece of soil and analyzing immediately. For each soil core, at least three analyses for each element on a macropore surface were performed. The matrix effect (de Vries and Vrebos, 2002) was eliminated by presenting the results in a semi-quantitative manner as the relative increase (RI) defined as:

$$RI = (C_{MS} - C_{IC})/C_{IC} \quad (1)$$

where C_{MS} is the concentration of a given element on the macropore surface and C_{IC} is the average reference concentration of the same element in all inner core samples. Average reference concentrations of the inner core samples were used since the differences in composition between the inner core samples were very low and most probably had a random character.

For micro-XRF mapping, an M4 Tornado μ-XRF (Bruker) was used to analyze a cut surface across an untreated macropore surface. The X-ray source was an Rh-tube at 50 kV, 600 mA, and no filter was used. Each point was measured for 50 ms and comprised a full energy dispersive spectrum that can be interpreted for qualitative and quantitative analyses. The sample chamber was set at 20 mbar pressure to facilitate analysis of light elements Na, Mg, Al, and Si (low energy lines).

2.5.4. Microbial community analyses

Microbial cells were isolated from the macropore surface and inner core samples according to an indirect DNA extraction method (Högfors-Rönnholm et al., 2018b). Partial 16S rRNA genes were amplified, the amplicons sequenced on the Illumina MiSeq platform (2 × 300 bp), and the downstream bioinformatics analyzed as reported in Högfors-Rönnholm et al. (2018a). Data interpretation and plotting was performed in R (v. 3.5.1; R Core Team, 2015) using the phyloseq package (v. 1.20; McMurdie and Holmes, 2013) and the taxonomy was assigned using the Silva NR database (Quast et al., 2013). The phylogenetic tree was constructed by FastTree (v. 2.1.8; Price et al., 2010) and drawn using iTOL (v. 4.2.1).

2.6. Eh-pH diagrams

The Eh-pH predominance diagram (Fig. 2) for Fe species was drawn using PhreePlot (http://www.phreeplot.org/). This software contains an embedded version 3 of the PHREEQC software (Parkhurst and Appelo, 2013). Equilibrium constants were those provided in the wateq4f database, dated 14 Feb. 2019, and supplied with the PhreePlot software. For schwertmannite the log K value of 18 was used for the solubility of the mean composition $Fe_8O_8(OH)_{4.8}(SO_4)_{1.6} + 20.8H^+ \rightarrow 8Fe^{3+} + 1.6SO_4^{2-} + 12.84H_2O$ (Bigham et al., 1996). Concentrations of solution species were average values measured in the drainage water from the reference parts of the field described by Dalhem et al. (2019). The

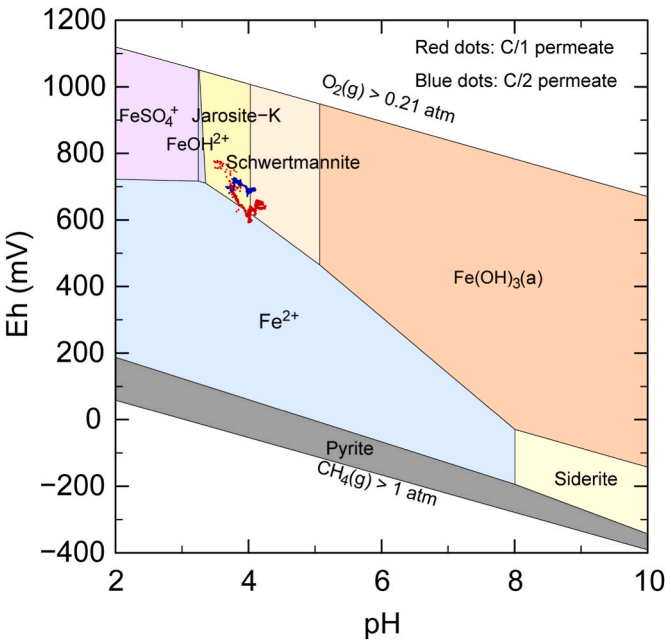

Fig. 2. Complete sets of recorded experimental pH and Eh results for the control permeates plotted in a Eh-pH diagram. The figure is a predominance diagram for the Fe species at 10 °C.

diagram is intended as a qualitative guidance only because of the estimates involved as well as the uncertainties in thermodynamic and structural information. The diagram is calculated for 10.0 °C, the temperature used in the experiments.

2.7. Statistical analyses

Non-parametric Mann–Whitney *U* test was used to determine significant differences ($p < 0.05$; IBM SPSS Statistics 25.0) in geochemical soil extract data and relative microbial abundances between treatments as well as between macropore surfaces and inner cores within the treatments. Alpha diversity was calculated as the Shannon diversity index. One-way ANOVA analysis followed by Tukey multiple comparison of means was used to determine significant differences ($p < 0.05$; R, v. 3.5.1) in alpha diversity between the control and treatments as well as between macropore surfaces and inner cores within the treatments. A principal coordinate analysis (PCoA) plot of beta diversity was calculated using the weighted UniFrac metric. To analyze the combined geochemical soil extract and 16S rRNA gene amplicon data, compositional principal component analysis (cPCA) biplots (R, v. 3.5.1) were used as previously described (Högfors-Rönnholm et al., 2018a). Due to experimental limitations resulting in two replicates for permeate measurements, only comparative analyses were performed on these results.

2.8. Data availability

Nucleic acid sequences have the NCBI BioProject accession number: PRJNA563865.

3. Results and discussion

3.1. Permeate characteristics and biogeochemical environment of control boreal ASS

3.1.1. Permeates

The pH and Eh values of the control permeates were largely constant during the experiment (Fig. 3a) and at the end of the experiment the pH was 4.1–4.2 and the Eh 655–695 mV. The stable pH was probably due to

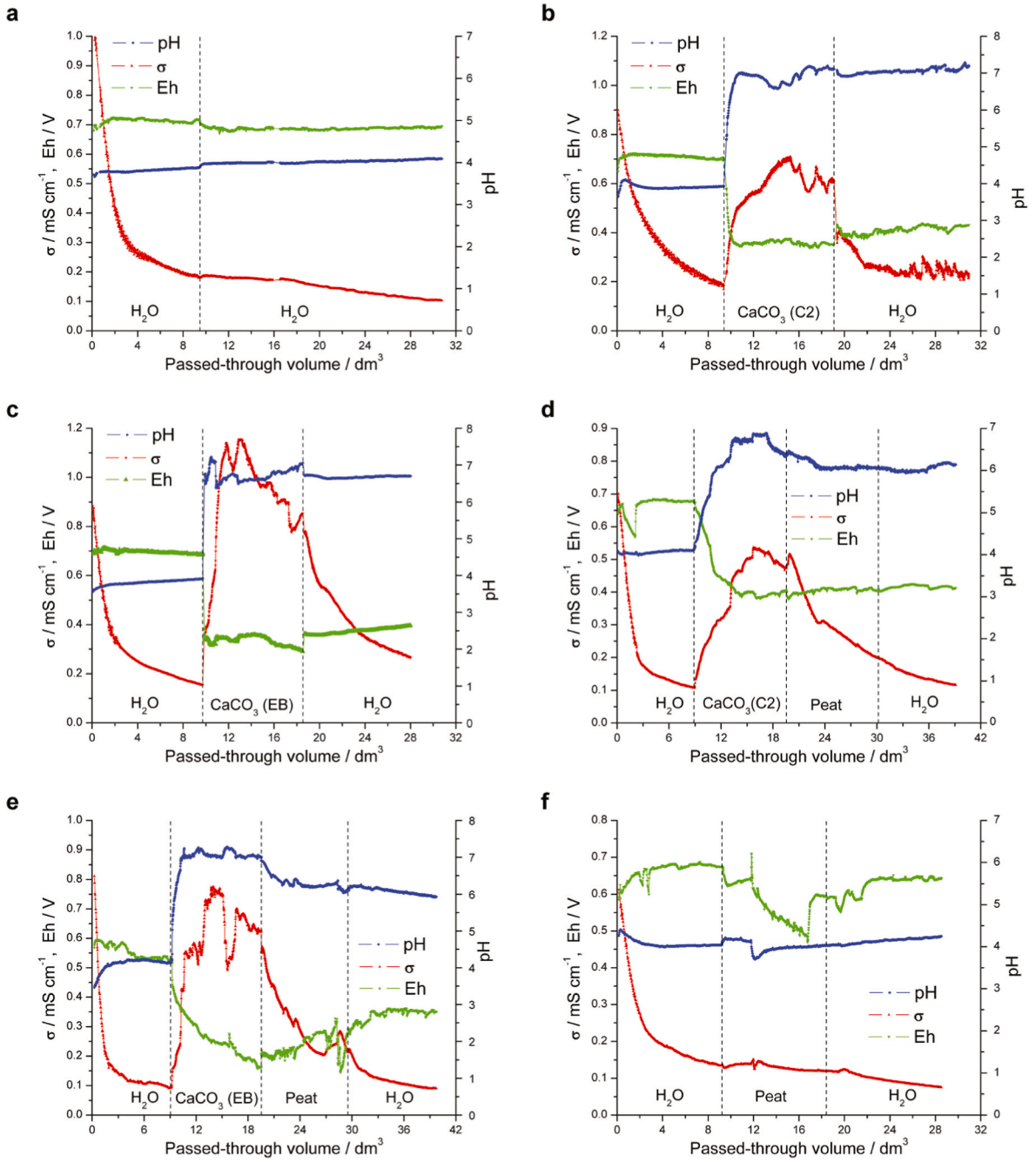

Fig. 3. Changes in pH, temperature-corrected (to 25 °C) conductivity (σ), and oxidation-reduction potential (Eh) (versus SHE) in permeates during passing water and suspensions of different substances through the soil core: a) MilliQ-ultrapure water; b) C2 $CaCO_3$ suspension; c) Enrich Bio $CaCO_3$ suspension; d) C2 $CaCO_3$ and peat suspension; e) Enrich Bio $CaCO_3$ and peat suspension; and f) peat suspension.

the buffering influence of reaction 2 (Wu et al., 2015), here modified to reflect a mean natural composition of schwertmannite $Fe_8O_8(OH)_{4.8}(SO_4)_{1.6}$ (Bigham et al., 1996):

$$8KFe_3(SO_4)_2(OH)_6 \rightleftharpoons 3Fe_8O_8(OH)_{4.8}(SO_4)_{1.6} + 14.4H^+ + 8K^+ + 11.2SO_4^{2-} + 9.6H_2O \quad (2)$$

The mean composition of schwertmannite was also used in the construction of the Eh-pH diagram in Fig. 2. Plotting Eh versus pH in a predominance diagram with respect to iron (Fig. 2), showed that the boundary between regions of predominance for jarosite and schwertmannite occurred at a pH value of 4. This strongly suggested a solution chemistry controlled by the relationship between the solution and two solid phases, jarosite and schwertmannite, both shown to be present on the macropore surfaces of the control soil core samples in a parallel publication (Yu et al., 2023). The role of jarosite as a buffering substance has been previously reported (Mosley et al., 2017; Trueman et al., 2020).

Even though the Eh of the system was likely a mixed potential involving several redox couples in disequilibria, the stability of the Eh indicates the presence of a redox poising capacity of the system (Grundl, 1994). As shown by Barcelona and Holm (1991), solids can contribute significantly to a system's redox poising capacity. Possible ferric species participating in the stabilization of a high Eh at a pH of 4.1–4.2 could be potassium jarosite and schwertmannite, the half-reactions being:

$$KFe_3(SO_4)_2(OH)_6 + 6H^+ + 3e^- \rightleftharpoons 3Fe^{2+} + 2SO_4^{2-} + K^+ + 6H_2O \quad (3)$$

$$Fe_8O_8(OH)_6SO_4 + 22H^+ + 8e^- \rightleftharpoons 8Fe^{2+} + SO_4^{2-} + 14H_2O \quad (4)$$

The presence of hydrogen ions in Eqs (3) and (4) indicates a significant coupling between pH buffering and redox poising (Grundl, 1994). Both jarosite (e.g., Chu et al., 2006; Keene et al., 2010; Kölbl et al., 2021) and schwertmannite (e.g., Paikaray, 2021; Schoepfer and Burton, 2021) can function as electron acceptors. Reaction products in the form of Fe^{2+}, K^+, and SO_4^{2-} were transported away by the percolating water flow (Table 1; Fig. 4a). However, schwertmannite is stabilized, at least in the short term, by adsorbing ions (Paikaray, 2021) that may accentuate the short-term role of jarosite as an electron acceptor (see also discussion on treatment effects below and results by Yu et al. (2023) where it is shown that it is mainly jarosite that is affected by the treatments). There is some accumulation of manganese on macropore surfaces (Table 2), but the concentrations were close to the detection limit and consequently the contribution of Mn to the Eh is likely minor. An important electron donor was the significant quantities of organic matter in the soil.

The soil core samples used in this work came from an agricultural field adjacent to the experimental field described by Dalhem et al. (2019) and was from a layer just above the drainage depth. The permeates thus passed through a similar network of preferential-flow macropores as the groundwater on its way to the subsurface drainage pipes under field conditions. For comparison, spring and fall measurements of the groundwater in the reference parts of the experimental field during the years 2015–2022 show an average pH of 3.82 ± 0.09 and Eh of 626.6 ± 26.2 mV (Dalhem et al., 2019 and unpublished results). The somewhat higher pH and Eh in the experiments described here was likely a consequence of the continuous flushing out of acid and dissolved reduced species.

During the experiment, the sulfate concentration decreased in the control permeates as the ions were flushed out with the water (Fig. 4a). The metal concentrations e.g., Al, Co, and Ni (Table 1) were highest in the control permeates and were similar to those in a previous study with a similar experimental setup (Wu et al., 2015). However, these metal concentrations were diluted due to the constant water flow through the preferential-flow macropores in these experiments and therefore much lower than those found under field conditions (Dalhem et al., 2019).

3.1.2. *Macropore surfaces*

The pH values of control macropore surface extracts were uniform at 3.7–3.8 (Fig. 5a) while the conductivity varied between 105 and 184 μS cm^{-1} (Fig. 5b). The former supported the hypothesis that pH was strongly buffered by schwertmannite and jarosite as discussed above. SO_4–S in the control macropore surface extracts (Fig. 5c) showed a median of 51 mg kg^{-1} that is common for ASS (e.g., Österholm and Åström, 2004). Dissolved Fe^{2+} was below the detection limit (i.e., <0.2 mg kg^{-1}) in the control macropore surface extracts (Fig. 5d), suggesting that immobilized iron at the preferential-flow macropore surfaces mainly occurred in the form of Fe^{3+} species.

The macro-XRF analysis showed an enrichment of S and, to a lesser degree Fe, on the control macropore surfaces (Table 2). This enrichment effect of S was also seen in the micro-XRF (Fig. S3) analyses where S was strongly enriched on control macropore surfaces together with Fe. Furthermore, in the macro-XRF analysis, K was not notably depleted despite having a similar mobility to the depleted Mg (Table 2). Thus, the surface-enrichment patterns of S and Fe, and the lack of depletion of K, strongly supported the hypothesis that these elements were largely mobilized from inner cores but retained on macropore surfaces due to formation of jarosite and other iron-sulfate minerals. The lower concentrations of Al and Si (Table 2), related to the (phyllo)silicates of the soil, further suggested that the macropore surfaces were covered by a layer of secondary material that lacks these elements but suppresses their X-ray fluorescence from beneath. In a related publication, the surface minerals were studied using chemical digestion methods as well as XAS techniques concluding that surface layers were dominated by schwertmannite and jarosite (Yu et al., 2023).

Data on extracted DNA, 16S rRNA gene reads, and operational taxonomic units (OTUs; 97% similarity) from the amplicon sequencing are provided in Table S1. All of the assigned 16S rRNA gene OTUs were within the Bacteria domain and those populations with >1% relative abundance represented eight phyla (Fig. S4). This matched the trend of Archaea species having a generally higher optimal growth temperature. However, it could also have been influenced by the known bias of the PCR primers towards Bacteria (Hugerth et al., 2014) as Archaea have been identified with metagenomics sequencing in boreal ASS (Högfors-Rönnholm et al., 2022). Similar to other ASS environments (Stroud et al., 2014; Su et al., 2017), Proteobacteria (37–55% relative abundance; Fig. S4) dominated the microbial community composition on the control macropore surfaces. The most abundant OTUs aligned to unassigned Gammaproteobacteria KF-JG30-C25 (22–49%; Figs. 6 and 7), recently identified in acid mine drainage (AMD; Arce-Rodríguez et al., 2019) and in homogenized ASS and thought to have sulfur-oxidizing capabilities (Högfors-Rönnholm et al., 2020). OTUs from the Ktedonobacteraceae family of phylum Chloroflexi were the second most abundant (9–33%; Fig. 6; Fig. S4), which were most similar to the uncultured JG30a-KF-32 identified from an Atacama Desert soil (Fig. 7; Lynch et al., 2012). Other identified OTUs most similar to taxa with known acidophilic and acid-tolerant species (Figs. 6 and 7) included unassigned Acidimicrobiia (5–25%), Acidobacteraceae subgroup 1 (4–6%), and *Metallibacterium* sp. of the Rhodanobacteraceae family (0.1–2%) (Brown et al., 2011; Santofimia et al., 2013; Ziegler et al., 2013).

Overall, the conditions on the control macropore surfaces reflected a completely oxidized environment that was inhabited by acidophilic and

Table 1
pH, oxidation-reduction potential Eh (versus SHE), conductivity (σ), and the concentration of selected ions and elements in the permeates from the soil cores at the end of the experiment. Abbreviations are replicate experiments according to C/1 & C/2, water only controls; C2/1 & C2/2, C2 $CaCO_3$ suspension; EB/1 & EB/2, Enrich Bio $CaCO_3$ suspension; C2–P/1 & C2–P/2, C2 $CaCO_3$ and peat suspension; EB-P/1 & EB-P/2, Enrich Bio $CaCO_3$ and peat suspension; and P/1 & P/2, peat suspension.

Soil core	pH	Eh	σ	SO_4^{2-}	S	Al	K	Na	Mn	Mg	Ca	Fe	Co	Ni
		mV	μS cm^{-1}	mg L^{-1}								μg L^{-1}		
C/1	4.2	655	80	20.1	8	0.8	1.3	1.1	0.11	1.3	2.7	40	4	16
C/2	4.1	695	103	24.2	9	0.8	1.9	1.3	0.15	1.6	2.8	50	6	53
C2/1	7.0	533	208	31.8	12	<0.1	0.8	0.5	0.05	1.1	37.9	<10	2	6
C2/2	7.2	432	232	29.4	11	<0.1	1.2	0.7	0.05	1.1	41.6	<10	<2	<5
EB/1	5.9	492	171	47.8	18	0.1	1.2	2.3	0.06	1.2	26.7	<10	3	16
EB/2	6.7	396	267	50.5	18	<0.1	1.3	2.0	0.05	1.4	48.4	<10	<2	<5
C2–P/1	5.2	415	91	29.3	11	0.3	1.2	1.3	0.08	1.4	10	<10	3	10
C2–P/2	6.1	413	116	20.8	8	<0.1	0.8	0.7	0.03	0.8	16.9	<10	2	<5
EB-P/1	5.9	349	90	23.7	9	<0.1	1.3	0.8	0.06	0.9	12.8	<10	3	8
EB-P/2	4.9	501	86	25.3	3	0.1	0.4	0.3	0.02	0.3	3.1	<10	<2	6
P/1	4.6	478	77	24.9	9	0.6	1.6	1	0.1	1.7	4.7	20	4	21
P/2	4.3	642	75	20.0	7	0.7	1.5	0.7	0.08	1.1	3.1	30	4	13

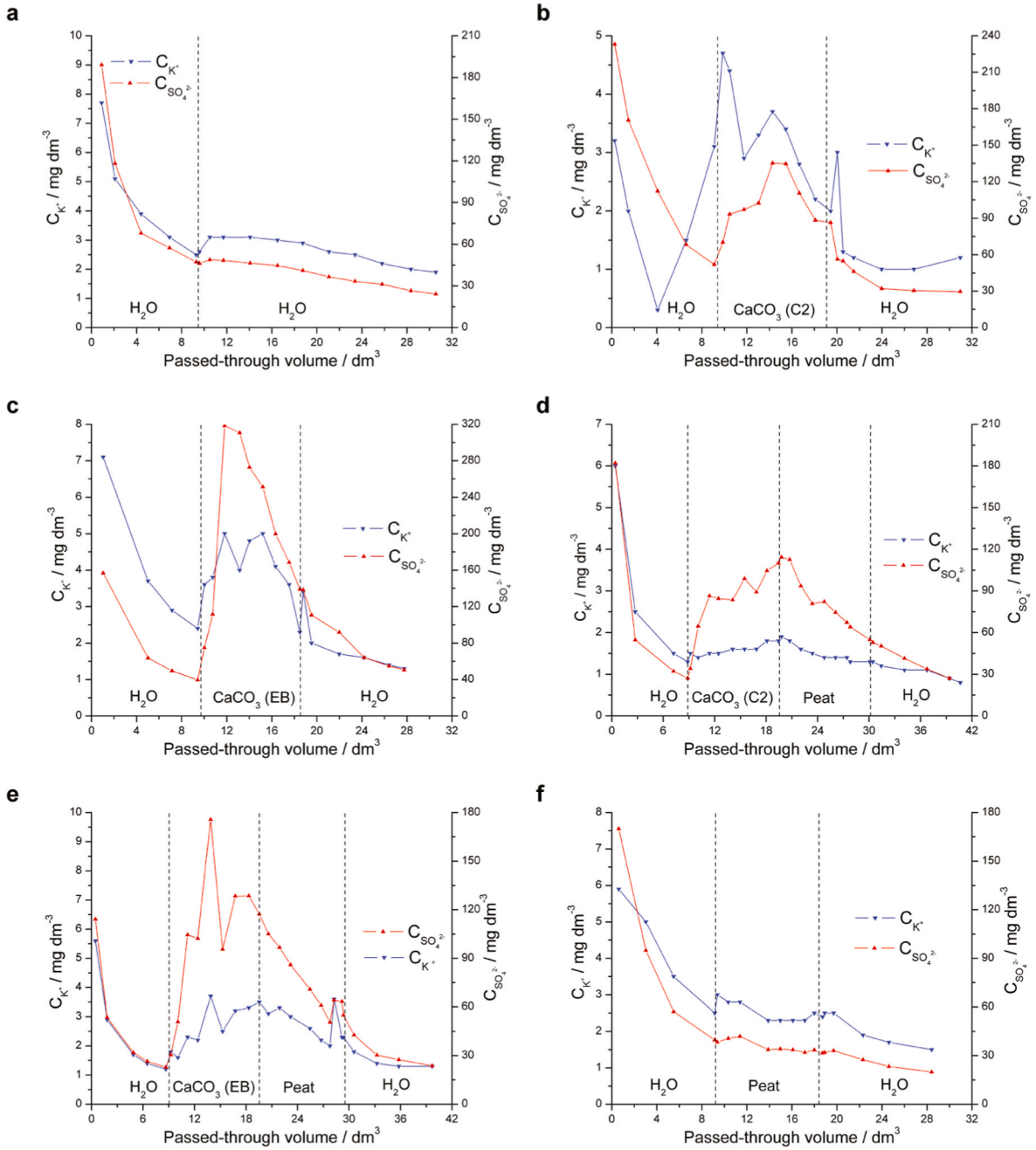

Fig. 4. Changes in concentration of sulfate ion (C_{SO4}) and concentration of potassium ion (C_K) in permeates during passing water and suspensions of different substances through the soil core: a) MilliQ-ultrapure water; b) C2 $CaCO_3$ suspension; c) Enrich Bio $CaCO_3$ suspension; d) C2 $CaCO_3$ and peat suspension; e) Enrich Bio $CaCO_3$ and peat suspension; and f) peat suspension.

acid-tolerant microorganisms equally well adapted to multiple environmental stresses as those found in AMD environments (Baker and Banfield, 2003) and in boreal ASS (Högfors-Rönnholm et al., 2022). In addition, these surfaces represent a pool of immobilized oxidation products in direct contact with percolating pore water where pH and redox conditions are governed by these compounds.

3.1.3. *Inner cores*

The pH of control inner core extracts was uniform at pH 3.7–3.8 (Fig. 5a) and the conductivity varied between 104 and 149 μS cm^{-1} (Fig. 5b), with no significant difference (Mann-Whitney *U* test, $p > 0.05$) to the control macropore surface extracts. The median value for SO_4–S in the control inner core extracts was slightly lower (median 42 mg kg^{-1}) although not significantly different ($p > 0.05$) than in the corresponding macropore surface extracts (Fig. 5c). The concentration of Fe^{2+} in the control inner core extracts was on average 0.5 mg kg^{-1} (Fig. 5d) and significantly higher ($p < 0.05$) than in control macropore surface extracts, indicating that inner cores served as a Fe^{2+} source. As ferrous iron diffuses towards a macropore surface it can be oxidized and included in solid ferric iron phases on the surface or if conditions allow, it can be taken up by pore water and transported away in a drainage flow, contributing to the relatively high (in comparison to the treatments) total Fe concentrations in the control permeate (Table 1).

No statistically significant difference was found in the microbial alpha diversity when comparing control macropore surface samples with inner core samples (one-way ANOVA plus Tukey posthoc test, $p > 0.05$; Fig. S5a) or in the beta diversity PcoA (Fig. S5b). The microbial community composition in the control inner core samples was also

Table 2
Relative increase (RI[a]) of elements on macropore surfaces compared to the same element in inner cores. Abbreviations are replicate experiments according to C/1 & C/2, water only controls; C2/1 & C2/2, C2 $CaCO_3$ suspension; EB/1 & EB/2, Enrich Bio $CaCO_3$ suspension; C2–P/1 & C2–P/2, C2 $CaCO_3$ and peat suspension; EB-P/1 & EB-P/2, Enrich Bio $CaCO_3$ and peat suspension; and P/1 & P/2, peat suspension.

Experiment	Mg	Al	Si	Mn	S	K	Ca	Fe
C/1	−0.95	−0.30	−0.30	0.00	26.13	−0.05	−0.07	0.65
C/2	−0.79	−0.31	−0.27	0.83	27.39	−0.05	−0.18	2.10
C2/1	−0.23	−0.29	−0.26	0.30	20.17	−0.10	0.28	1.57
C2/2	−0.30	−0.39	−0.34	0.34	3.73	−0.06	3.08	0.85
EB/1	−0.78	−0.16	−0.18	0.14	10.52	−0.01	0.23	0.64
EB/2	−0.67	−0.20	−0.18	0.46	10.25	−0.04	0.68	1.71
C2–P/1	−0.67	−0.21	−0.15	0.30	8.17	0.07	0.12	0.74
C2–P/2	−0.72	−0.17	−0.20	0.34	11.06	−0.02	0.20	1.15
EB-P/1	−0.90	−0.35	−0.39	0.21	32.62	−0.21	−0.09	1.53
EB-P/2	−0.59	−0.14	−0.14	0.05	8.42	0.05	0.19	0.60
P/1	−0.55	−0.15	−0.11	0.09	8.08	0.01	−0.01	0.45
P/2	−0.34	−0.12	−0.10	0.16	6.74	0.01	−0.04	0.51

[a] RI = 0 means no change, RI > 0 means accumulation of the element on the surface, RI < 0 means depletion of the element on the surface.

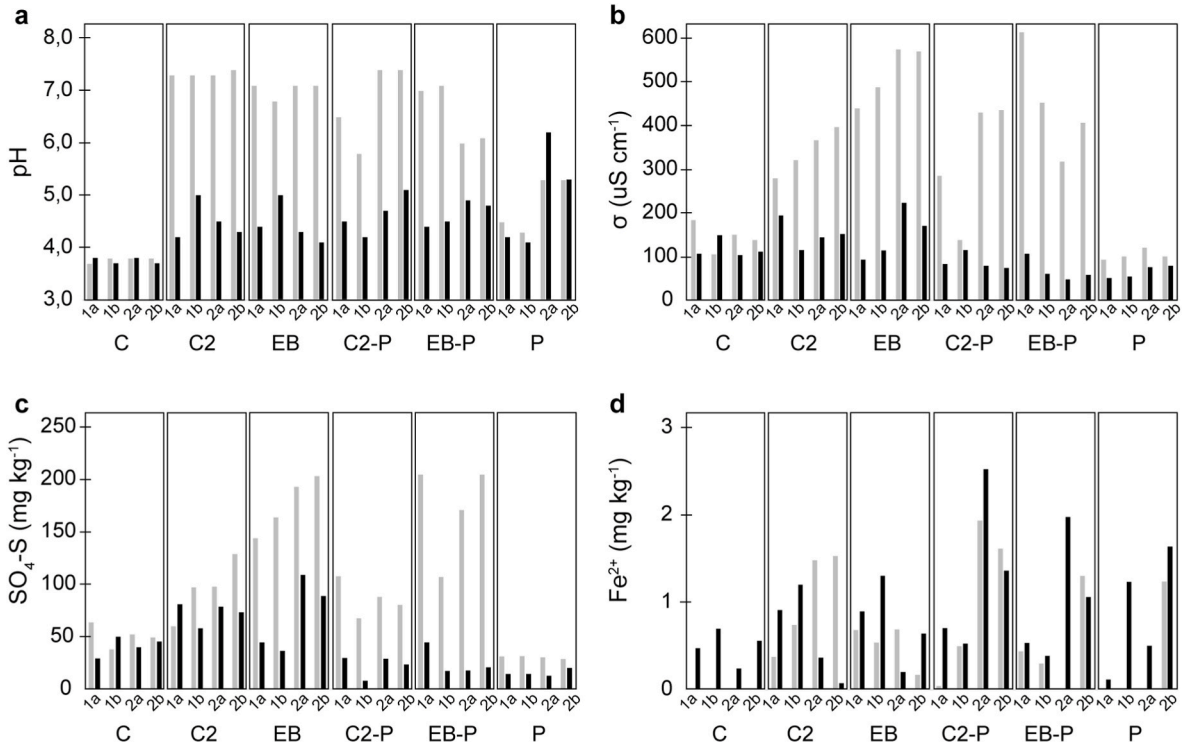

Fig. 5. pH (a), conductivity (σ; b), SO_4–S (c), and ferrous iron (d) in soil extracts of ASS control samples along with treated soil columns. The experiments were carried out in duplicates with the x-axis abbreviations: C, water only controls; C2, C2 $CaCO_3$ suspension; EB, Enrich Bio $CaCO_3$ suspension; C2–P, C2 $CaCO_3$ and peat suspension; EB-P, Enrich Bio $CaCO_3$ and peat suspension; and P, peat suspension. All analyses were carried out on duplicate samples from macropore surfaces (grey bars) and inner cores (black bars) from replicate treatments, giving four measurements per treatment (1a, 1b; duplicate samples from replicate 1 and 2a, 2b; duplicate samples from replicate 2).

dominated by Proteobacteria (53–69% relative abundance; Fig. 6), especially by OTUs belonging to the unassigned Gammaproteobacteria KF-JG30-C25 family (43–59%; Fig. 6). Other abundant OTUs were the same as in the control macropore surface samples, such as OTUs from the Ktedonobacteraceae family (6–30%), unassigned Acidimicrobiia (3–12%), Acidobacteraceae, subgroup 1 (2–5%), and from the Rhodanobacteraceae family (0.2–0.7%; Fig. 6).

Overall, the conditions in the control inner cores reflected a partially oxidized environment and suggested that ASS inner cores gradually leached sulfuric acid and ferrous iron to the environment, in part by way of macropore surface solid phases, and in part by directly entering percolating macropore flow.

3.2. Mitigation effects after treatment of boreal ASS

3.2.1. Permeates

After C2, EB, C2–P, and EB-P treatments, the permeates showed an increased pH (likely due to H^+ ion consumption; Eq. (5)) and conductivity (Table 1, Fig. 3b–e).

$$CaCO_3 + 2H^+ \rightleftharpoons Ca^{2+} + H_2O + CO_2 \quad (5)$$

The slightly lesser pH increase in permeates from C2–P and EB-P treatments compared to C2 and EB treatments (Table 1) likely reflected the lower $CaCO_3$ concentration in these treatment suspensions. The decrease in permeate Eh in C2, EB, C2–P, and EB-P treatments (Table 1, Fig. 3b–e) was similar to that found in drainage water from fields treated with $CaCO_3$ suspensions (Dalhem et al., 2019). This

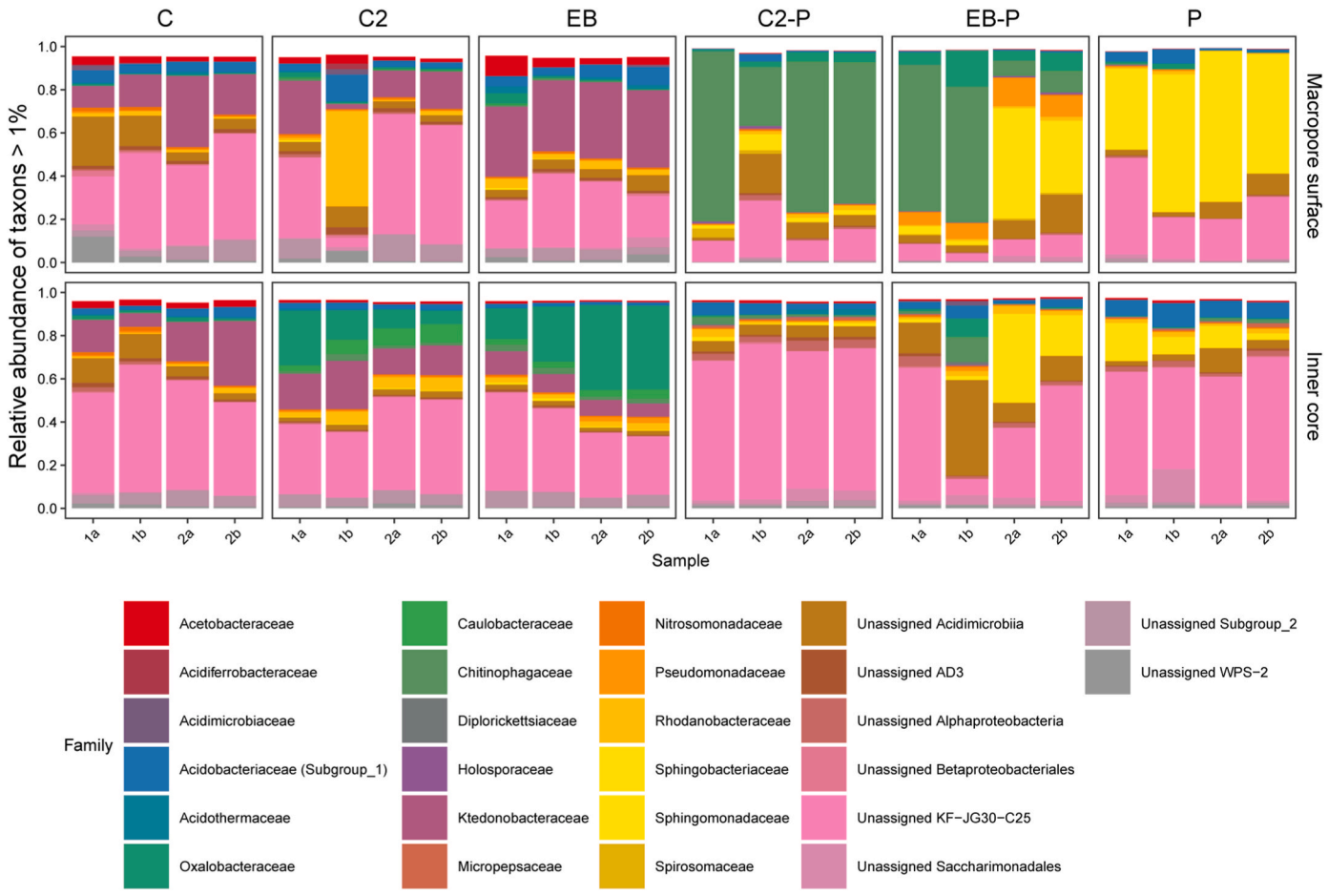

Fig. 6. Microbial community structure (>1% relative abundance) on family level. Abbreviations are replicate experiments according to C, water only controls; C2, C2 $CaCO_3$ suspension; EB, Enrich Bio $CaCO_3$ suspension; C2–P, C2 $CaCO_3$ and peat suspension; EB-P, Enrich Bio $CaCO_3$ and peat suspension; and P, peat suspension. All 16S rRNA gene amplicon sequencing was carried out on duplicate biological replicates from macropore surfaces and inner cores from replicate treatments, giving four stacked bars per treatment (1a, 1b; duplicate samples from replicate 1 and 2a, 2b; duplicate samples from replicate 2).

treatment-induced drop in Eh indicated a change in the main redox couple in the system. In fact, the pH increase brought about by C2, EB, C2–P, and EB-P treatments most likely converted jarosite into a Fe(III) oxyhydroxide such as lepidocrocite in treatments with $CaCO_3$, and ferrihydrite in treatments involving peat (Vithana et al., 2015; Kölbl et al., 2021; Yu et al., 2023):

$$KFe_3(OH)_6(SO_4)_2 \rightleftharpoons 3FeOOH + K^+ + 2SO_4^{2-} + 3H^+ \quad (6)$$

The drop in Eh coincided with the elimination of jarosite from macropore surfaces, but a possible casual connection remains to be established.

The resulting Eh after treatments, 349–533 mV (Table 1), was below the stability region of schwertmannite (Fig. 2), and the conclusion is that schwertmannite remaining on the macropore surfaces was largely stable both towards reduction and pH-induced transformation under the conditions and timescale of these experiments. The treatments also brought about a sharp decrease in iron in solution (Table 1). This may be due to the pH increase, favoring the formation of ferric oxyhydroxides if a suitable electron acceptor was available (assuming dissolved iron is largely in the ferrous form and has to be oxidized before forming ferric oxyhydroxide). However, as is discussed below regarding the macropore surfaces, surface adsorption of Fe^{2+} was clearly taking place. The P treatment resulted in only a minor permeate pH increase but a decrease in Eh in one replicate compared to the control permeates (Table 1, Fig. 3f), suggested a possible reducing effect by the P treatment. The SO_4^{2-} and K^+ concentrations, as well as the conductivity, in the permeates from the C2, EB, C2–P, and EB-P treatments strongly increased after the change from water to $CaCO_3$ suspension (Fig. 3b–e, 4b-e), indicating a mobilization of SO_4^{2-} and K^+. No increase in SO_4^{2-} and K^+ concentrations or conductivity was seen after addition of peat in the C2–P and EB-P treatments or in the P treatment (Fig. 3d–f, 4d-f). The decrease in total Fe concentrations observed in the permeates after C2, EB, C2–P, and EB-P treatments (Table 1) agreed with Eqs (2) and (6)), i.e., iron was immobilized while sulfate was mobilized. Metal concentrations, e.g., Al, Mn, Co, and Ni also decreased in the permeates after C2, EB, C2–P, and EB-P treatments (Table 1). The decrease in permeate metal concentrations in the C2 and EB treatments was likely due to the pH increase that decreased the solubility of metal hydroxides and carbonates (Palko and Weppling, 1994) and due to the adsorption of metal ions onto minerals (e.g., calcite) that further decreased metal ion mobility (Al et al., 2000). In the C2–P and EB-P treatments, the decrease in permeate metal concentrations was most likely due to both the pH increase and the metal retention capacity of the peat (Högfors-Rönnholm et al., 2018a, 2020). However, since the cation exchange capacity of peat is considerably decreased at low pH (Puustjarvi and Robertson, 1975), the P treatment alone only affected the permeate metal concentrations moderately, with a slight decrease in Fe and Mn concentrations (Table 1).

Overall, the quality of the permeates was improved by the treatments. After treatments containing only $CaCO_3$, permeates showed pH values close to neutral and low metal concentrations and Eh values were low. After combined treatments with $CaCO_3$ and peat, the increase in pH was more moderate while Eh and metal concentrations were still low.

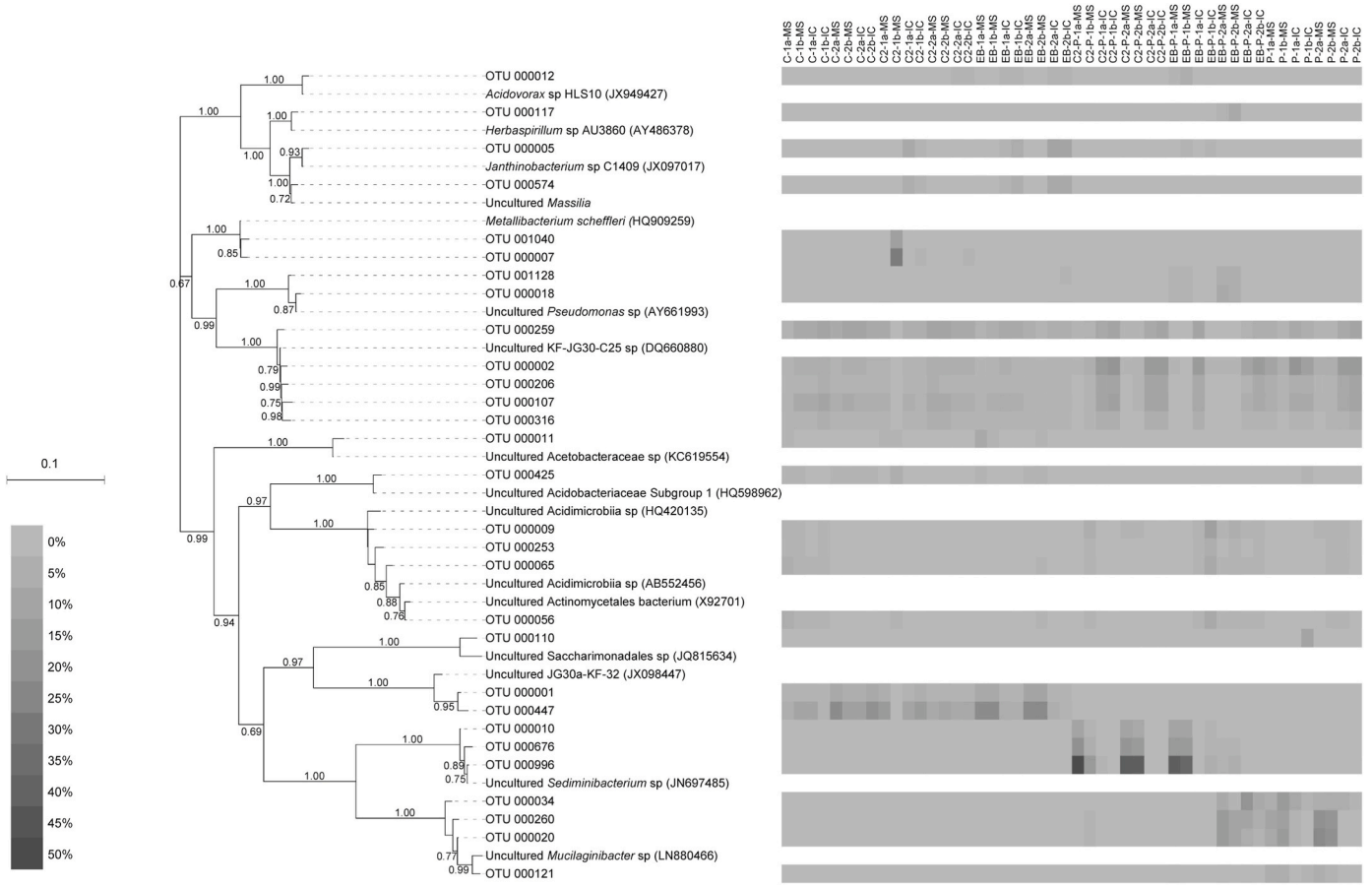

Fig. 7. Maximum likelihood (unrooted) phylogenetic tree (100 × bootstrap) and heat map of reference sequences from the NCBI database along with OTUs (>5% relative abundance) from the 16S rRNA gene sequencing. Abbreviations are replicate experiments according to C, water only controls; C2, C2 $CaCO_3$ suspension; EB, Enrich Bio $CaCO_3$ suspension; C2–P, C2 $CaCO_3$ and peat suspension; EB-P, Enrich Bio $CaCO_3$ and peat suspension; and P, peat suspension. All amplicon sequencing was carried out on duplicate biological replicates from macropore surfaces (MS) and inner cores (IC) from replicate treatments (1a, 1b; duplicate samples from replicate 1 and 2a, 2b; duplicate samples from replicate 2). Grey scale denotes percentage relative abundance of the OTUs and the scale bar gives the number of substitutions per site.

Pure peat treatments had only a minor effect on pH, Eh, and metal concentrations within the timescale of the experiments.

3.2.2. *Macropore surfaces*

Surfaces of preferential-flow macropores were directly accessible to the flowing solutions/suspensions and treatment effects on both chemistry and microbiology were clearly detectable. After the experiments, it was evident that both $CaCO_3$ and peat particles readily adsorbed to the macropore surfaces (Fig. 1b). The accessible surface area of the highly porous and heterogeneous macropore surface may be larger for the comparatively small $CaCO_3$ particle diameter (median 0.3 μm) used in the EB treatment as compared to the C2 treatment (median particle diameter 2.5 μm). The smaller particles may be able to reach otherwise inaccessible parts in the form of micropores of the macropore surface.

After all treatments, there was a significant (Mann-Whitney *U* test; $p < 0.05$) pH increase in macropore surface extracts to 7.3–7.4 for C2, 6.8–7.1 for EB, 5.8–7.4 for C2–P, 6.0–7.1 for EB-P, and pH 4.3–5.3 for P as compared to the control macropore surface extracts (Fig. 5a). The slightly lower extract pH seen in treatments involving EB as compared to treatment involving C2, may be due to a much larger surface area and thus, more jarosite/schwertmannite accessible to the EB suspension. The acidification accompanying the SO_4–S mobilization that follows jarosite conversion to Fe(III) oxyhydroxide (Eq. (6)) may be responsible for this. A pure P treatment raised the pH in the permeate and the macropore surface extract above that of the peat suspension (pH 3.8) itself. A pH increase was also observed in a long-term incubation experiment with dried and milled common reed leaf mixed into ASS (Michael et al., 2015). The EB, C2–P, and EB-P treatments showed a significant ($p < 0.05$) increase of SO_4–S in macropore surface extracts (medians of 178, 84, and 188 mg kg^{-1}, respectively) compared to control macropore surface extracts (Fig. 5c). The median SO_4–S after C2 treatment was higher (median of 97 mg kg^{-1}), but not significantly different ($p > 0.05$) from the untreated samples due to large within treatment variation (Fig. 5c). A similar SO_4–S mobilization effect was seen when C2 and EB were mixed with homogenized ASS (Högfors-Rönnholm et al., 2018a, 2020). Once again, the smaller particle size may explain why treatments with EB were much more efficient in mobilizing SO_4–S than treatment with C2. On the other hand, the P treatment showed a significant ($p < 0.05$) decrease of SO_4–S in macropore surface extracts (median of 30 mg kg^{-1}) compared to control macropore surface extracts (Fig. 5c). Significantly increased ($p < 0.05$) Fe^{2+} concentrations were found in macropore surface extracts after C2, EB, and C2–P treatments compared to control macropore surface extracts (Fig. 5d). There was an indication that EB-P and P treatments may increase Fe^{2+} concentrations but the difference was not statistically significant due to the large within treatment variations (Fig. 5d). The mobilization of Fe^{2+} in surface extracts was surprising. The macropore surface is an environment where ferric iron is expected to dominate, as was the case in the control macropores. However, as ultrafine-grained $CaCO_3$ is adsorbed onto macropore surfaces, ferrous iron will be scavenged from the pore water and adsorbed and/or precipitated onto the $CaCO_3$ particles (Al et al., 2000). The effects of the C2, EB, C2–P, and EB-P treatments were also observed

in the macro-XRF analysis of macropore surfaces (Table 2). There was a decreased surface accumulation of S at the macropore surfaces, compared to controls, while the Fe accumulation remained approximately the same. This is in agreement with the results by Yu et al. (2023), where jarosite is shown to have been largely converted to lepidocrocite. The minor increase of calcium at the macropore surfaces after C2, EB, C2–P, and EB-P treatments was probably due to some residual $CaCO_3$ adsorption (even though areas without visible adsorption were chosen for these analyses). On the other hand, in the P treatments there was a decreased surface accumulation for both Fe and S (Table 2) compared to the controls. This may reflect the electron-donating capacity of peat (Aeschbacher et al., 2012) in combination with a relatively stable pH which contributed to some reductive dissolution of ferric surface layers during the treatments thus mobilizing both S and Fe (Eqs (3) and (4)).

No statistically significant differences ($p > 0.05$) were found in the microbial community alpha diversities when comparing macropore surface samples of the C2 and EB treatments with control macropore surface samples (Fig. S5a). In the beta diversity, only variation over the second minor axis could be seen (Fig. S5b). On the macropore surfaces of the C2 and EB treatments, Proteobacteria (29–63% relative abundance; Fig. S4) and Chloroflexi (6–37% relative abundance) dominated the relative community composition with the most abundant OTUs aligning to KF-JG30-C25 (4–55%) and JG30a-KF-32 (2–36%; Fig. 6), respectively. These relative abundances did not differ significantly ($p > 0.05$) from the relative abundances of the same OTUs found in the macropore surface samples of the control. Other OTUs found on control macropore surfaces were also identified on the macropore surfaces of the C2 and EB treatments, such as *Metallibacterium* sp. (0.1–44%), unassigned Acidimicrobiia (3–13% abundance), and the Acidobacteraceae, subgroup 1 (2–12%; Figs. 4 and 5). These relative abundances did not either differ significantly ($p > 0.05$) from the relative abundances of the same OTUs found on the control macropore surfaces, suggesting a similar microbial composition on control and on C2 and EB treated macropore surfaces although they were found to have diverse geochemical environments.

However, statistically significant differences ($p < 0.05$) were found in the alpha diversities when comparing macropore surface samples of the C2–P, EB-P, and P treatments with control macropore surface samples (Fig. S5a). In the beta diversity, variation over the first major axis could also be seen (Fig. S5b) and the relative community composition on the C2–P, EB-P and P treated macropore surfaces were dominated by members of phylum Bacteroidetes (37–84% relative abundance; Fig. S4) instead of Proteobacteria. In all macropore surface samples of the C2–P and EB-P treatments, the relative abundances of the KF-JG30-C25 OTUs were considerably decreased (3–26%) compared to the control macropore surfaces (Fig. 6). However, this decrease was only significant ($p < 0.05$) in the EB-P treatment compared to the control. On the macropore surfaces of the C2–P and EB-P treatments, Chitinophagaceae family OTUs aligning to uncultured *Sediminibacterium* sp. (7–79%; Figs. 6 and 7; Katsaveli et al., 2012), and Sphingobacteriaceae family OTUs, aligning to uncultured *Mucilaginibacter* sp. (0.1–50%; Figs. 6 and 7) previously identified in AMD in Svalbard (García-Moyano et al., 2015) were significantly increased ($p < 0.05$) compared to the control. A possible explanation for the shift from a control macropore surface KF-JG30-C25 dominated community to a C2–P and EB-P macropore surface *Sediminibacterium* sp. dominated community could be the latter species' growth at neutral pH values utilizing the abundant organic acids in peat as electron donors (Kang et al., 2014; Reddy and DeLaune, 2008) coupled to the toxicity of pH values > 5 and organic acids to acidophiles (Fang and Zhou, 2006; Högfors-Rönnholm et al., 2018a). It should be noted that the relative abundance of Chitinophagaceae and Sphingobacteriaceae OTUs found in the peat were negligible (data not shown) and that these species were also found in the control, C2, and EB treatments suggested the peat itself was an unlikely source for these OTUs. The conditions on the C2–P and EB-P macropore surfaces were also favorable for other neutrophiles (microorganisms with a near neutral pH optimum for growth) such as OTUs from the Oxalobacteraceae (1–17% in C2–P and EB-P samples) and Pseudomonadaceae (6–13% in EB-P samples) families (Fig. 6). The C2–P and EB-P treatments of macropore surfaces were therefore sufficient to alter the microbial communities away from acidophiles likely to catalyze PASS oxidation (Wu et al., 2013; Högfors-Rönnholm et al., 2022). On the macropore surfaces of the P treatments, *Mucilaginibacter* sp. (37–70% relative abundance) of the Sphingobacteriaceae family and KF-JG30-C25 group (19–45%) OTUs were dominant (Figs. 6 and 7). This indicated that *Mucilaginibacter* sp., which are low temperature chemo-organotrophic species that tolerate slightly acidic environments (Männistö et al., 2010), were able to utilize a carbon source in the peat (Pankratov et al., 2007). Although the geochemical data indicated some Fe^{3+} reduction on the macropore surfaces of the P treatments, no known iron-reducing bacteria could be identified. This was most likely because the taxonomy assignment method used in this study was unable to assign all OTUs on a species level.

The key driver that divided the macropore surface samples over the first major axis in the cPCA biplot was the presence of peat (Fig. 8a). The macropore control and P treatment surface samples were further separated from the C2, EB, C2–P, and EB-P treated macropore surface samples over the second minor axis by pH, Fe^{2+}, and conductivity links directed towards the C2, EB, C2–P, and EB-P treated samples. C2–P and EB-P treated macropore surface samples were furthermore separated from P treated samples over the second minor axis by *Sediminibacterium* sp. and *Mucilaginibacter* sp. links.

3.2.3. Inner cores

The treatments affected the macropore surfaces considerably, which led to a difference between inner cores and macropore surfaces regarding concentrations of e.g., H^+ and SO_4–S (Fig. 5). These differences were not found in the untreated controls. As a result, steep concentration gradients between macropore surfaces and inner cores were formed by the treatments, both directly and indirectly. Direct effects can be e.g., the neutralization reaction in Eq. (5) establishing a pH gradient and ion-exchange effects. Indirect effects are induced transformations such as Eq. (6) where an equilibrium is massively disturbed by the treatments. The new gradients may, at least temporarily, reverse the direction of diffusional transport of some substances between inner cores and macropore surfaces.

There was a moderate, but significant ($p < 0.05$) pH increase in inner core extracts after all treatments compared to the control inner core extracts (Fig. 5a) with pH 4.2–5.1 for C2, pH 4.1–5.0 for EB, 4.2–5.1 for C2–P, 4.4–4.9 for EB-P, and 4.1–6.2 for P. However, in contrast to the close agreement between macropore surface and inner core pH values in the controls, the pH of C2, EB, C2–P, and EB-P treated macropore surfaces were significantly ($p < 0.05$) higher than the pH of corresponding inner cores. No significant ($p > 0.05$) difference was found in pH between P treated macropore surfaces and inner cores (Fig. 5a). This indicated that the $CaCO_3$ component of the C2, EB, C2–P, and EB-P treatments was able to initially increase the pH of the macropore surfaces considerably and secondarily moderately increase the pH of inner cores. The effect on inner cores would be through diffusion, a much slower process, and therefore moderate on the time scale of these experiments.

The median values for SO_4–S in all treated inner core extracts, except for the C2 treatment, were significantly lower ($p > 0.05$) than in the corresponding macropore surface extracts (Fig. 5c). However, the C2 treatment showed a significant ($p < 0.05$) increase of SO_4–S (median 76 mg kg^{-1}), while the EB treatment showed no significant increase of SO_4–S (median 67 mg kg^{-1}) in inner core extracts compared to control inner core extracts (Fig. 5c). The SO_4–S in C2–P and EB-P treated inner cores (median 29 and 19 mg kg^{-1}, respectively) were not significantly different compared to control inner cores. In contrast, the P treatment showed a significant ($p < 0.05$) decrease of SO_4–S in inner core extracts (median 14 mg kg^{-1}) compared to control inner core extracts (Fig. 5c).

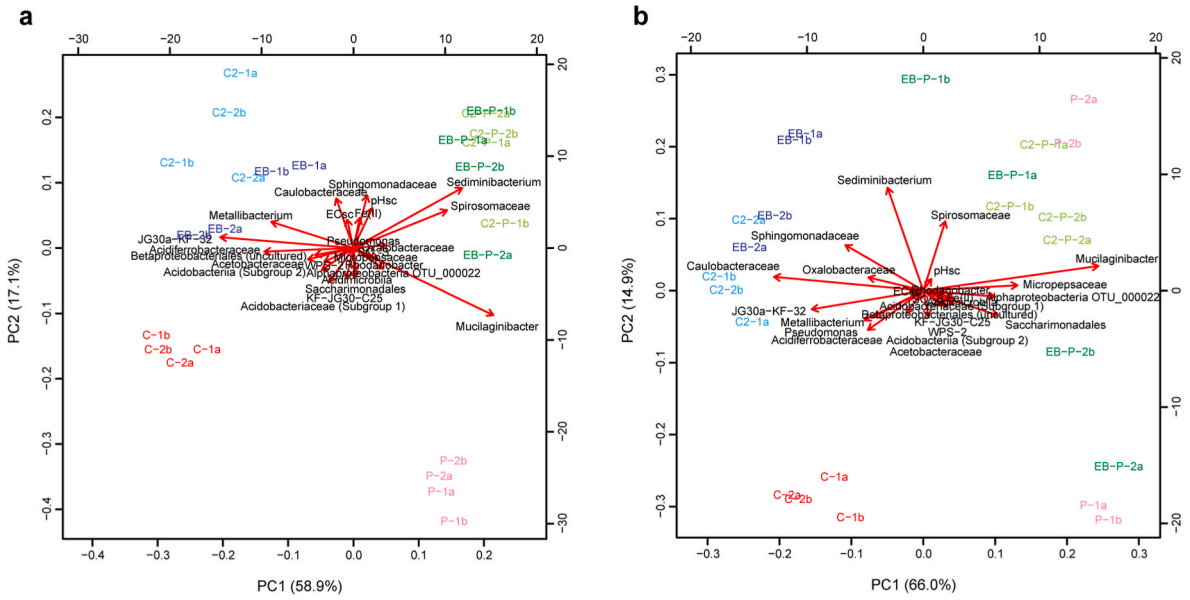

Fig. 8. Biplot from the compositional principal component analysis of the soil geochemical and microbiological parameters from a) macropore surface and b) inner core control samples (C, red), macropore surface samples treated with $CaCO_3$ suspension (C2, light blue), Enrich Bio $CaCO_3$ suspension (EB, blue), C2 $CaCO_3$ and peat suspension (C2–P, light green), Enrich Bio $CaCO_3$ and peat suspension (EB-P, green) and peat suspension (P, pink). All geochemical and microbiological analyses were performed on duplicate samples from replicate treatments, resulting in four samples per treatment (1a, 1b; duplicate samples from replicate 1, and 2a, 2b; duplicate samples from replicate 2).

As SO_4–S was mobilized at the surfaces in treatments with $CaCO_3$, the direction of the diffusional transport of sulfur was likely temporarily reversed due to the formed concentration gradient. This may explain the increased SO_4–S concentrations in the inner cores. Earlier work with homogenized ASS (Högfors-Rönnholm et al., 2018a, 2020) showed SO_4–S mobilization in connection with C2, EB, and C2–P treatments. As the major SO_4–S mobilization effect in this work was seen in C2, EB, C2–P, and EB-P treated macropore surface samples but less so in inner core samples, the present study confirmed that the main source of the mobilized SO_4–S was the sulfur that had accumulated on the ASS macropore surfaces. This was in agreement with results of Yu et al. (2023) showing the near-complete conversion of jarosite to Fe(III) oxyhydroxide.

Interestingly, peat inhibited this phenomenon, and even contributed to a decrease of SO_4–S in inner cores of the P treatments. Presently it is not possible to say whether the decrease in SO_4–S was due to sulfate reduction as, with the methods used in this study, no known sulfate reducing bacteria could be identified in the soil from P treated inner cores as discussed below. No statistically significant difference ($p > 0.05$) was found when comparing Fe^{2+} concentrations in the C2, EB, C2–P, EB-P, and P treated inner core extracts (Fig. 5d) to Fe^{2+} concentrations in the control inner core extracts. Nor was a statistically significant difference found in the Fe^{2+} concentrations when comparing C2, EB, C2–P, EB-P, and P treated inner core samples with corresponding macropore surface samples.

No statistically significant differences were found in the microbial alpha diversities when comparing C2, EB, C2–P, EB-P, and P treatment inner core samples to control inner core samples ($p > 0.05$; Fig. S5a). However, in the beta diversity biplot (Fig. S5b), variation over the first major axis was observed and the relative community composition in the EB-P and P treated inner cores were less dominated by members of phylum Proteobacteria (26–73% relative abundance; Fig. S4) than in the control and C2, EB, and C2–P treated inner cores (53–80%). A significant difference was also found in the microbial alpha diversity when comparing C2–P treated macropore surface samples with corresponding inner core samples ($p < 0.05$; Fig. S5a). For the other treatments, no significant difference ($p > 0.05$) in the microbial alpha diversity could be found when comparing macropore surface samples to corresponding inner core samples.

Just as on the macropore surfaces of the C2 and EB treatments, the relative microbial community composition of C2 and EB treated inner cores was dominated by OTUs aligning to the unassigned Gammaproteobacteria KF-JG30-C25 family (27–46%) and the JG30a-KF-32 from the Ktedonobacteraceae family (6–22%; Fig. 6). These relative abundances did not differ significantly ($p > 0.05$) from the relative abundances of the same OTUs found in the control inner cores, which indicated that the pH increase caused by the C2 and EB treatments (Fig. 3a) had no substantial impact on the relative abundance of the KF-JG30-C25 population inhabiting the macropore surfaces nor the inner cores of the ASS. However, other dominating OTUs belonging to the Oxalobacteraceae family (6–39%) and the Caulobacteraceae family (2–8%; Fig. 6) were found in C2 and EB treated inner cores. These relative abundances were significantly higher ($p < 0.05$) compared to the relative abundances of the same OTUs found in the control inner cores. The Oxalobacteraceae OTUs aligned most closely to taxa living in pH neutral soils (Fig. 7; Garrity et al., 2015). Species of the Caulobacteraceae family are chemo-organotrophs that can be found in a range of habitats, e.g., in soil (Abraham et al., 2014). The relative microbial community composition of the C2–P, EB-P, and P treated inner cores were dominated by OTUs aligning to the unassigned KF-JG30-C25 family (7–72%) and the unassigned Acidimicrobiia (2–47%; Fig. 6). The KF-JG30-C25 relative abundances in the EB-P and P treated inner cores did not differ significantly ($p > 0.05$) from the relative abundances found in the control inner cores. However, the KF-JG30-C25 relative abundances were significantly higher ($p < 0.05$) in the C2–P treated inner cores compared to the control inner cores. The relative abundances of the Acidimicrobiia OTUs in the C2–P, EB-P and P treated inner cores did not differ significantly ($p > 0.05$) from the relative abundances found in the control inner cores. Other dominating OTUs belonging to *Mucilaginibacter* sp. (0.3–41%) and Acidobacteraceae subgroup 1 (2–6%; Figs. 5 and 6) were also found in the C2–P, EB-P, and P treated inner cores. Although the P treatments decreased SO_4–S leaching from inner cores, no known sulfate reducing bacteria could be identified. This was most likely because the taxonomy assignment method used in this study was unable to assign all OTUs on a species level. The results from the inner cores suggested that, although the pH increase in the samples did

not affect the relative abundance of most abundant acidophilic bacterial populations present, the low abundance populations were affected. It can thereby be concluded that as in AMD environments (Kuang et al., 2013), pH was highly important in structuring the overall boreal ASS microbial community.

In the cPCA biplot, the inner core extract variables (i.e., pH, σ, Fe^{2+}, and SO_4–S) were close to the center of the biplot (Fig. 8b) indicating that the geochemical environment was similar in all inner cores. The key driver that divided the inner core samples over the first major axis in the cPCA biplot was the presence of peat. The inner cores are not directly accessible via macropores and instead transport into and out from the inner cores is dominated by diffusion (Yong, 2003). It was therefore not surprising that treatment effects on chemical species and populations of microorganisms were mild at the time scale of this work. However, a statistically significant pH increase in C2, EB, C2–P, EB-P, and P treated inner core extracts showed that transport was indeed taking place. An increase in SO_4–S in inner core extracts with C2 and EB treatments indicated that treatments mainly targeting macropore surfaces and mobilizing SO_4–S there, also affected inner cores. It was likely that mobilized SO_4–S diffused from the surface into the inner core. Peat had a negative effect on SO_4–S concentrations of inner core extracts, irrespective of whether SO_4–S had been mobilized at the surface (C2–P and EB-P treatments) or if SO_4–S had been diminished at the surface (P treatment).

These facts, in combination with a lack of mobilized SO_4–S in the permeate after a P treatment and evidence of a conversion of jarosite to Fe(III) oxyhydroxide (which should mobilize SO_4–S) shown by Yu et al. (2023), point towards a possible sulfate reduction. However, as no sulfate-reducing bacteria could be identified in this work, the exact mechanism behind this reduction in SO_4–S concentrations is presently unknown.

4. Conclusions

This study presents novel data regarding the diverse biogeochemical properties of macropore surfaces and inner cores of a boreal ASS. The results highlight the all-important role of the macropore surface in a mature ASS and in the control experiments showed a remarkable stability of both pH and Eh of the pore water. It is hypothesized that the stability was provided by solid compounds on the macropore surfaces. Future studies must provide estimates of the contribution to the pH buffering capacity as well as the redox poising capacity of these macropore-surface compounds. This information is of relevance especially in the planning of a remediation of acid sulfate soils by flooding, treatment with alkaline amendments, and/or supplying electron donors in the form of organic matter.

The main properties of ASS drain water are thus determined by the macropore surfaces it has been in contact with. This leads to the conclusion that methods aimed at mitigating the negative environmental effects of ASS drainage must target the soil macropore surfaces. In this work, it has been shown that macropore surfaces can be targeted by passing a suspension of $CaCO_3$ and/or peat through the system of preferential-flow macropores in the soil. Microbial community analysis suggested a shift towards species typically growing at circumneutral pH on the treated macropore surfaces but a largely unchanged community within the soil inner cores.

Declaration of competing interest

The authors declare that they have no known competing financial interests or personal relationships that could have appeared to influence the work reported in this paper.

Data availability

Data will be made available on request.

Acknowledgements

Authors E.H.-R., P.S., T.L., P.Ö., and S.E. received funding from the European Agricultural Fund for Rural Development via the Rural Development Programme for Mainland Finland 2014–2020 through the Centre for Economic Development, Transport and the Environment in Ostrobothnia [grant numbers 10308 and 101851]. E.H.-R. received additional funding from Aktiastiftelsen i Vasa. S.E. further received funding from Handlanden Gustaf Svanljungs Donationsfond, Oiva Kuusisto Säätiö and Aktiastiftelsen i Vasa. Author M.D. received funding from The Swedish Research Council Formas [grant number 2018-00760] and the Geological Survey of Sweden [grant number 36-1878/2017]. Nordkalk and Vapo Fibers, Finland are acknowledged for providing $CaCO_3$ and peat, respectively. Timo Riikonen, Jussi Hyvönen, Bernard Klu, and Julien Walser are thanked for laboratory assistance. Professor Mats Åström is thanked for fruitful discussions.

Appendix A. Supplementary data

Supplementary data to this article can be found online at https://doi.org/10.1016/j.apgeochem.2023.105779.

References

Abraham, W.R., Rohde, M., Bennasar, A., 2014. The family Caulobacteraceae. In: Rosenberg, E., DeLong, E.F., Lory, S., Stackebrandt, E., Thompson, F. (Eds.), The Prokaryotes. Springer, Berlin, Heidelberg, pp. 179–205.
Aeschbacher, M., Graf, C., Schwarzenbach, R.P., Sander, M., 2012. Antioxidant properties of humic substances. Environ. Sci. Technol. 46, 4916–4925.
Al, T.A., Martin, C.J., Blowes, D.W., 2000. Carbonate-mineral/water interactions in sulfide-rich mine tailings. Geochem. Cosmochim. Acta 64, 3933–3948.
Andriesse, J.P., 1988. Nature and Management of Tropical Peat Soils. Food and Agriculture Organization of United Nations, Rome, Italy.
Arce-Rodríguez, A., Puente-Sánchez, F., Avendaño, R., Libby, E., Mora-Amador, R., Rojas-Jimenez, K., Pieper, D.H., Chavarría, M., 2019. Untapped microbial composition along a horizontal oxygen gradient in a Costa Rican volcanic influenced acid rock drainage system. bioRxiv, 663633.
Åström, M., Österholm, P., Bärlund, I., Tattari, S., 2007. Hydrochemical effects of surface liming, controlled drainage and lime-filter drainage on boreal acid sulfate soils. Water Air Soil Pollut. 179, 107–116.
Baker, B.J., Banfield, J.F., 2003. Microbial communities in acid mine drainage. FEMS Microbiol. Ecol. 44, 139–152.
Barcelona, M.J., Holm, T.R., 1991. Oxidation-reduction capacities of aquifer solids. Environ. Sci. Technol. 25, 1565–1572.
Bates, R.G., 1973. Determination of pH, second ed. John Wiley & Sons, p. 335.
Bigham, J.M., Schwertmann, U., Traina, S.J., Winland, R.L., Wolf, M., 1996. Schwertmannite and the chemical modeling of iron in acid sulfate waters. Geochem. Cosmochim. Acta 60, 2111–2121.
Boman, A., Åstrom, M., Fröjdö, S., 2008. Sulfur dynamics in boreal acid sulfate soils rich in metastable iron sulfide – the role of artificial drainage. Chem. Geol. 255, 68–77.
Brown, J.F., Jones, D.S., Mills, D.B., Macalady, J.L., Burgos, W.D., 2011. Application of a depositional facies model to an acid mine drainage site. Appl. Environ. Microbiol. 77, 545–554.
Chu, C., Lin, C., Wu, Y., Lu, W., Long, J., 2006. Organic matter increases jarosite dissolution in acid sulfate soils under inundation conditions. Aust. J. Soil Res. 44, 11–16.
Dalhem, K., Engblom, S., Stén, P., Österholm, P., 2019. Subsurface hydrochemical precision treatment of a coastal acid sulfate soil. Appl. Geochem. 100, 352–362.
Dang, T., Mosley, L.M., Fitzpatrick, R., Marschner, P., 2016. Addition of organic material to sulfuric soil can reduce leaching of protons, iron and aluminium. Geoderma 271, 63–70.
de Vries, J.L., Vrebos, A.R., 2002. In: Van Grieken, R.E., Markowicz, A.A. (Eds.), Handbook of X-Ray Spectrometry. Marcel Dekker Inc., New York, Basel.
Dent, D., 1986. Acid Sulphate Soils: a Baseline for Research and Development, vol. 39. ILRI publication, Wageningen, the Netherlands.
Fadrus, H., Malý, J., 1975. Suppression of iron(III) interference in the determination of iron(II) in water by the 1,10-phenanthroline method. Analyst 100, 549–554.
Fang, D., Zhou, L.X., 2006. Effect of sludge dissolved organic matter on oxidation of ferrous iron and sulfur by *Acidithiobacillus ferrooxidans* and *Acidithiobacillus thiooxidans*. Water, Air, Soil Pollut. 171, 81–94.
García-Moyano, A., Austnes, A.E., Lanzén, A., González-Toril, E., Aguilera, Á., Øvreås, L., 2015. Novel and unexpected microbial diversity in acid mine drainage in Svalbard (78° N), revealed by culture-independent approaches. Microorganisms 3, 667–694.
Garrity, G.M., Bell, J.A., Lilburn, T., 2015. Oxalobacteraceae fam. nov. In: Brenner, D.J., Krieg, N.R., Staley, J.T. (Eds.), Bergey's Manual of Systematics of Archaea and Bacteria. Springer, New York, p. 623.
Grundl, T., 1994. A review of the current understanding of redox capacity in natural, disequilibrium systems. Chemosphere 28, 613–626.

Hinwood, A.L., Horwitz, P., Appleyard, S., Barton, C., Wajrak, M., 2006. Acid sulphate soil disturbance and metals in groundwater: implications for human exposure through home grown produce. Environ. Pollut. 143, 100–105.
Högfors-Rönnholm, E., Christel, S., Dalhem, K., Lillhonga, T., Engblom, S., Österholm, P., Dopson, M., 2018a. Chemical and microbiological evaluation of novel chemical treatment methods for acid sulfate soils. Sci. Total Environ. 625, 39–49.
Högfors-Rönnholm, E., Christel, S., Engblom, S., Dopson, M., 2018b. Indirect DNA extraction method suitable for acidic soil with high clay content. MethodsX 5, 136–140.
Högfors-Rönnholm, E., Christel, S., Lillhonga, T., Engblom, S., Österholm, P., Dopson, M., 2020. Biodegraded peat and ultrafine calcium carbonate results in retained metals and higher microbial diversities in boreal acid sulfate soil. Soil Ecol. Lett. 2, 120–130.
Högfors-Rönnholm, E., Lundin, D., Brambilla, D., et al., 2022. *Gallionella* and *Sulfuricella* populations are dominant during the transition of boreal potential to actual acid sulfate soils. Commun. Earth Environ. 3, 304. https://doi.org/10.1038/s43247-022-00642-z.
Hugerth, L.W., Wefer, H.A., Lundin, S., Jakobsson, H.E., Lindberg, M., Rodin, S., Engstrand, L., Andersson, A.F., 2014. DegePrime, a program for degenerate primer design for broad-taxonomic-range PCR in microbial ecology studies. Appl. Environ. Microbiol. 80, 5116–5123.
Johnston, S.G., Slavich, P., Hirst, P., 2004. The acid flux dynamics of two artificial drains in acid sulfate soil backswamps on the Clarence River floodplain, Australia. Aust. J. Soil Res. 42, 623–637.
Johnston, S., Hirst, P., Slavich, P., Bush, R., Aaso, T., 2009. Saturated hydraulic conductivity of sulfuric horizons in coastal floodplain acid sulfate soils: variability and implications. Geoderma 151, 387–394.
Joukainen, S., Yli-Halla, M., 2003. Environmental impacts and acid loads from deep sulfidic layers of two well-drained acid sulfate soils in western Finland. Agric. Ecosyst. Environ. 95, 297–309.
Kang, H., Kim, H., Lee, B.I., Joung, Y., Joh, K., 2014. *Sediminibacterium goheungense* sp. nov., isolated from a freshwater reservoir. Int. J. Syst. Evol. Microbiol. 64, 1328–1333.
Katsaveli, K., Vayenas, D., Tsiamis, G., Bourtzis, K., 2012. Bacterial diversity in Cr(VI) and Cr(III)-contaminated industrial wastewaters. Extremophiles 16, 285–296.
Keene, A., Johnston, S., Bush, R., Sullivan, L., Burton, E., 2010. Reductive dissolution of natural jarosite in a tidally inundated acid sulfate soil: geochemical implications. In: 19th World Congress of Soil Science, Soil Solutions for a Changing World, pp. 100–103, 1–6 August 2010, Brisbane, Australia.
Kölbl, A., Marschner, P., Mosley, L., Fitzpatrick, R., Kögel-Knabner, I., 2018. Alteration of organic matter during remediation of acid sulfate soils. Geoderma 332, 121–134.
Kölbl, A., Kaiser, K., Winkler, P., Mosley, L., Fitzpatrick, R., Marschner, P., Wagner, F.E., Häusler, W., Mikutta, R., 2021. Transformation of jarosite during simulated remediation of a sandy sulfuric soil. Sci. Total Environ. 773, 145546.
Kuang, J., Huang, L., Chen, L., et al., 2013. Contemporary environmental variation determines microbial diversity patterns in acid mine drainage. ISME J. 7, 1038–1050.
Lynch, R.C., King, A.J., Farías, M.E., Sowell, P., Vitry, C., Schmidt, S.K., 2012. The potential for microbial life in the highest-elevation (> 6000 m.a.s.l.) mineral soils of the Atacama region. J. Geophys. Res. 117 https://doi.org/10.1029/2012JG001961.
Männistö, M.K., Tiirola, M., McConnell, J., Häggblom, M.M., 2010. *Mucilaginibacter frigoritolerans* sp. nov., *Mucilaginibacter lappiensis* sp. nov. and *Mucilaginibacter mallensis* sp. nov., isolated from soil and lichen samples. Int. J. Syst. Evol. Microbiol. 60, 2849–2856.
McMurdie, P.J., Holmes, S., 2013. phyloseq: an R package for reproducible interactive analysis and graphics of microbiome census data. PLoS One 8, e61217. https://doi.org/10.1371/journal.pone.0061217.
Michael, P.S., Fitzpatrick, R., Reid, R., 2015. The role of organic matter in ameliorating acid sulfate soils with sulfuric horizons. Geoderma 255–256, 42–49.
Mosley, L.M., Biswas, T.K., Cook, F.J., Marschner, P., Palmer, D., Shand, P., Yuan, C., Fitzpatrick, R.W., 2017. Prolonged recovery of acid sulfate soils with sulfuric materials following severe drought: causes and implications. Geoderma 308, 312–320.
Nordmyr, L., Boman, A., Åström, M., Österholm, P., 2006. Estimation of leakage of chemical elements from boreal acid sulfate soils. Boreal Environ. Res. 11, 261–273.
Nordmyr, L., Åström, M., Peltola, P., 2008. Metal pollution of estuarine sediments caused by leaching of acid sulphate soils. Estuar. Coast Shelf Sci. 76, 141–152.
Nordstrom, D.K., Jenne, E.A., Ball, J.W., 1979. Redox equilibria of iron in acid mine waters. In: Jenne, E.A. (Ed.), Chemical Modeling in Aqueous Systems, ACS Symposium Series, vol. 93, pp. 51–79. Washington, D.C.
Österholm, P., Åström, M., 2004. Quantification of current and future leaching of sulfur and metals from Boreal acid sulfate soils, western Finland. Aust. J. Soil Res. 42, 547–551.
Paikaray, S., 2021. Environmental stability of schwertmannite: a Review. Mine Water Environ. 40, 570–586.
Palko, J., Weppling, K., 1994. Lime requirement experiments in acid sulphate soils. Acta Agric. Scand. Sect. B Soil Plant Sci 44, 149–156.
Pankratov, T.A., Tindall, B.J., Liesack, W., Dedysh, S.N., 2007. *Mucilaginibacter paludis* gen. nov., sp. nov. and *Mucilaginibacter gracilis* sp. nov., pectin-, xylan- and laminarin-degrading members of the family Sphingobacteriaceae from acidic Sphagnum peat bog. Int. J. Syst. Evol. Microbiol. 57, 2349–2354.
Parkhurst, D.L., Appelo, C.A.J., 2013. Description of input and examples for PHREEQC version 3–A computer program for speciation, batch-reaction, one-dimensional transport, and inverse geochemical calculations. U.S. Geol. Surv. Techniq. Methods, Book 6, 6–43. Chapter A43.
Price, M.N., Dehal, P.S., Arkin, A.P., 2010. FastTree 2–approximately maximum-likelihood trees for large alignments. PLoS One 5, e9490. https://doi.org/10.1371/journal.pone.0009490.
Puustjarvi, V., Robertson, R.A., 1975. Physical and chemical properties. In: Robinson, D. W., Lamb, J.G.D. (Eds.), Peat in Horticulture. Academic Press, London, pp. 23–38.
Quast, C., Pruesse, E., Yilmaz, P., Gerken, J., Schweer, T., Yarza, P., Peplies, J., Glockner, F.O., 2013. The SILVA ribosomal RNA gene database project: improved data processing and web-based tools. Nucleic Acids Res. 41, D590–D596. https://doi.org/10.1093/nar/gks1219.
R Core Team, 2015. The R Project for Statistical Computing. http://www.r-project.org/. (Accessed 6 April 2020).
Reddy, K.R., DeLaune, R.D., 2008. Biogeochemistry of Wetlands: Science and Application. CRC Press, Boca Raton.
Roos, M., Åström, M., 2006. Gulf of Bothnia receives high concentrations of potentially toxic metals from acid sulphate soils. Boreal Environ. Res. 11, 383–388.
Santofimia, E., González-Toril, E., López-Pamo, E., Gomariz, M., Amils, R., Aguilera, A., 2013. Microbial diversity and its relationship to physicochemical characteristics of the water in two extreme acidic pit lakes from the Iberian Pyrite Belt (SW Spain). PLoS One 8, e66746. https://doi.org/10.1371/journal.pone.0066746.
Schoepfer, V.A., Burton, E.D., 2021. Schwertmannite: a review of its occurrence, formation, structure, stability and interactions with oxyanions. Earth Sci. Rev. 221, 103811.
Stroud, J.L., Low, A., Collins, R.N., Manefield, M., 2014. Metal(loid) bioaccessibility dictates microbial community composition in acid sulfate soil horizons and sulfidic drain sediments. Environ. Sci. Technol. 48, 8514–8521.
Su, J.-Q., Xia, Y., Yao, H.-Y., Li, Y.-Y., An, X.-L., Singh, B.K., Zhang, T., Zhu, Y.-G., 2017. Metagenomic assembly unravel microbial response to redox fluctuation in acid sulfate soil. Soil Biol. Biochem. 105, 244–252.
Sullivan, L.A., Bush, R.T., Fyfe, D.M., 2002. Acid sulfate soil drain ooze: distribution, behaviour and implications for acidification and deoxygenation of waterways. In: Lin, M.M.C., Sullivan, L.A. (Eds.), Acid Sulfate Soils in Australia and China. Science Press, Beijing, p. 91.
Trueman, A.M., McLaughlin, M.J., Mosley, L.M., Fitzpatrick, R.W., 2020. Composition and dissolution kinetics of jarosite-rich segregations extracted from an acid sulfate soil with sulfuric material. Chem. Geol. 543, 119606.
Virtanen, S., 2015. Redox reactions and water quality in cultivated boreal acid sulphate soils in relation to water management. PhD Thesis. University of Helsinki, Helsinki. http://urn.fi/URN. ISBN:978-951-51-1519-5.
Vithana, C.L., Sullivan, L.A., Burton, E.D., Bush, R.T., 2015. Stability of schwertmannite and jarosite in an acidic landscape: prolonged field incubation. Geoderma 239–240, 47–57.
Wu, X., Wong, Z.L., Sten, P., Engblom, S., Österholm, P., Dopson, M., 2013. Microbial community potentially responsible for acid and metal release from an Ostrobothnian acid sulfate soil. FEMS Microbiol. Ecol. 84, 555–563.
Wu, X., Sten, P., Engblom, E., Nowak, P., Österholm, P., Dopson, M., 2015. Impact of mitigation strategies on microbial community from an Ostrobothnian acid sulfate soil. Sci. Total Environ. 526, 215–221.
Yli-Halla, M., Virtanen, S., Mäkelä, M., Simojoki, A., Hirvi, M., Innanen, S., Mäkelä, J.J., Sullivan, L., 2017. Abundant stocks and mobilization of elements in boreal acid sulfate soils. Geoderma 308 (Suppl. C), 333–340.
Yong, R.N., 2003. Influence of microstructural features on water, ion diffusion and transport in clay soils. Appl. Clay Sci. 23, 3–13.
Yu, C., Högfors-Rönnholm, E., Stén, P., Engblom, S., Åström, M.E., 2023. Iron-sulfur geochemistry and acidity retention in hydrologically active macropores of boreal acid sulfate soils: effects of mitigation suspensions of fine-grained calcite and peat. Sci. Total Environ. 856, 159142.
Ziegler, S., Waidner, B., Itoh, T., Schumann, P., Spring, S., Gescher, J., 2013. *Metallibacterium scheffleri* gen. nov., sp. nov., an alkalinizing gammaproteobacterium isolated from an acidic biofilm. Int. J. Syst. Evol. Microbiol. 63, 1499–1504.